

Carrier-phase Two-Way Satellite Frequency Transfer over a Very Long Baseline

M Fujieda¹, D Piester², T Gotoh¹, J Becker², M Aida¹ and A Bauch²

¹National Institute of Information and Communications Technology, Koganei, Japan

²Physikalisch-Technische Bundesanstalt (PTB), Bundesallee 100, 38116 Braunschweig, Germany

E-mail: miho@nict.go.jp

Abstract.

In this paper we report that carrier-phase two-way satellite time and frequency transfer (TWSTFT) was successfully demonstrated over a very long baseline of 9,000 km, established between the National Institute of Information and Communications Technology (NICT) and the Physikalisch-Technische Bundesanstalt (PTB). We verified that the carrier-phase TWSTFT (TWCP) result agreed with those obtained by conventional TWSTFT and GPS carrier-phase (GPSCP) techniques. Moreover, a much improved short-term instability for frequency transfer of 2×10^{-13} at 1 s was achieved, which is at the same level as previously confirmed over a shorter baseline within Japan. The precision achieved was so high that the effects of ionospheric delay became significant which are ignored in conventional TWSTFT even over a long link. We compensated for these effects using ionospheric delays computed from regional vertical total electron content maps. The agreement between the TWCP and GPSCP results was improved because of this compensation.

1. Introduction

There is a need for synchronization between remote clocks in radio astronomy, particle accelerators, and metrology [1, 2, 3]. With the development of highly accurate optical clocks and an increase in the number of simultaneously controlled instruments, there has been a corresponding increase in the required accuracy for time and frequency transfer. Recently, there have been extensive studies regarding time and frequency transfer over optical fibers [4, 5, 6]. Time synchronization based on an Ethernet-based network has been developed to realize sub nanosecond accuracy [7]. Moreover, optical frequency dissemination through optical fiber links enables the comparison of remote optical clocks and the measurement of the absolute transition frequency with reference to a remote cesium fountain clock without any limitations with respect to its accuracy [8, 9]. The transfer length exceeded 900 km [10].

Optical fiber links may be established for time and frequency transfer among various institutes located within the same continental region. However, it will be challenging to establish intercontinental optical fiber links. To make overseas connections, the utilization of satellite links such as GPS and two-way satellite time and frequency transfer (TWSTFT) will be indispensable, and there is a need to improve their measurement precision and accuracy [11, 12]. These techniques have been adopted since 1999 for the determination of Coordinate Universal Time (UTC) and International Atomic Time (TAI) [13]. Practically all institutes that maintain time and frequency standards adopt GPS time and frequency transfer to become part of the network of institutes collaborating in the realization of TAI with the BIPM. The use of GLONASS and Galileo has become more and more common practice, but in this paper we limit ourselves to use GPS frequency transfer in parallel to carrier-phase TWSTFT (TWCP). In addition, some institutes also use TWSTFT as a method that is independent of GPS. Unfortunately, the measurement precision has not significantly improved since its implementation many years ago [14]. This is mainly due to the high costs for the lease of large bandwidths of transponder capacity on communication satellites.

Both TWSTFT and GPS utilize phase-modulated signals with pseudo-random noise codes, and the code phase has been used to measure propagation time. The Coarse/Acquisition (C/A) code rate and carrier frequency of the GPS L1 signal are 1.023 Mega chip-per-second (cps) and 1.57542 GHz, respectively [15]. The measurement precision realized by the C/A code is about 10 ns with an averaging time of 13 min for time transfer. With the implementation of GPS carrier-phase measurements (GPSCP), the precision was improved to several tens of picoseconds. On the other hand, a code rate of 2.5 Mcps is typically used in TWSTFT. The measurement precision (jitter) for 1-second data points is about 0.5 ns when taken with a carrier-to-noise density ratio of 55 dBHz [16]. In the case where the carrier-phase measurement is implemented at about 10 GHz, we can expect the measurement precision to be improved by three orders of magnitude. Schäfer et al. introduced the use of the carrier phase to TWSTFT [17] and Fonville et al. demonstrated an intercontinental test result for a few hours [18]. The

National Institute of Information and Communications Technology (NICT) confirmed that the result obtained using TWCP agreed with that of GPSCP over a short baseline of 100 km [11]. After this regional exercise, we performed a more ambitious TWCP experiment over one of the longest baselines worldwide with the intention to evaluate the error sources that would be otherwise negligible over a short baseline. Our target is to improve the measurement precision of TWSTFT in intercontinental links. This study covers availability, error sources, and uncertainty over a longer baseline for TWCP. First, we introduce the time difference using carrier-phase information. Next, we discuss the experimental equipment, results, and discussions. Finally, we present our conclusions.

2. Description of carrier-phase two-way satellite frequency transfer

Two Earth stations, A and B, work as a pair. Four sets of phase information are required to describe the time difference by TWCP using a commercial geostationary satellite because we have four unknown values: the time difference between the two stations, the phase fluctuation induced by the translation of the received to the transmitted signal at the satellite, and two geometrical distances between the satellite and the two stations involved. Each station transmits a signal and detects the phases of its own transmitted signal and that of the signal received from the counterpart station.

Uplink and downlink signal angular frequencies are expressed as ω_u and ω_d , respectively; times of the reference clocks at station A and B are expressed as $\tau_a(t)$ and $\tau_b(t)$ in seconds, respectively; angular frequency of the translation onboard oscillator is expressed as $\omega_s = \omega_u - \omega_d$; time of the onboard clock is expressed as $\tau_s(t)$ in seconds. When a transmitted signal from station A, $\sin(\omega_u t + \omega_u \tau_a(t))$, arrives at the satellite, it shifts to $\sin(\omega'_u t + \omega_u \tau_a(t))$ because of the Doppler effect. Here ω'_u is given with the radial velocity $v_a(t)$ from station A to the satellite as

$$\omega'_u = \omega_u \left(1 - \frac{v_a(t)}{c}\right) \quad (1)$$

Here c is the speed of light. The signal is down-converted by the onboard signal $\sin(\omega_s t + \omega_s \tau_s(t))$ to $\sin[(\omega'_u - \omega_s)t + \omega_u \tau_a(t) - \omega_s \tau_s(t)]$. When this signal arrives at station B, it shifts to $\sin(\omega''_d t + \omega_u \tau_a(t) - \omega_s \tau_s(t))$ because of the Doppler effect. Using a local signal $\sin(\omega_d t + \omega_d \tau_b(t))$ at station B, the received signal is finally down-converted to $\sin[(\omega''_d - \omega_d)t + \omega_u \tau_a(t) - \omega_s \tau_s(t) - \omega_d \tau_b(t)]$. The angular frequency received at station B with the Doppler shift is expressed with the radial velocity $v_b(t)$ from station B to the satellite as

$$\omega''_d = (\omega'_u - \omega_s) \left(1 - \frac{v_b(t)}{c}\right) = \omega_d - \omega_d \frac{v_b(t)}{c} - \omega_u \frac{v_a(t)}{c} + \omega_u \frac{v_a(t)}{c} \frac{v_b(t)}{c} \quad (2)$$

In the case of a geostationary satellite, the quantity of $v(t)/c$ is in the range of 10^{-8} to 10^{-9} . Thus, it is thought that the fourth term on the right hand is less than 10^{-16} and negligible. To simplify the description, it is eliminated hereafter. The phase information of the signal includes the ionospheric and tropospheric delays along the signal path multiplied by the signal angular frequency including the Doppler shift. Considering the

small magnitude of $v(t)/c$ we neglect the effects of the Doppler shifts in the ionospheric and tropospheric delays. Accordingly, the phase information $\phi_{ab}(t)$ in radian of the signal which is transmitted from station A and received at station B is given by

$$\begin{aligned}\phi_{ab}(t) &= \omega_u \tau_a(t) - \omega_s \tau_s(t) - \omega_d \tau_b(t) - (\omega_u v_a(t)t + \omega_d v_b(t)t)/c \\ &\quad + \omega'_u I_{ua}(t) + \omega''_d I_{db}(t) + \omega'_u T_a(t) + \omega''_d T_b(t) + \omega_u \frac{v_a(t)}{c} \frac{v_b(t)}{c} t \\ &\approx \omega_u \tau_a(t) - \omega_s \tau_s(t) - \omega_d \tau_b(t) - (\omega_u \rho_{as}(t) + \omega_d \rho_{bs}(t))/c \\ &\quad + \omega_u I_{ua}(t) + \omega_d I_{db}(t) + \omega_u T_a(t) + \omega_d T_b(t)\end{aligned}\quad (3)$$

Here ρ_{as} and ρ_{bs} are the geometrical distances between the satellite and stations A and B, respectively. T_a and T_b are tropospheric delays in seconds which are frequency independent over stations A and B, respectively. I_{ij} is the ionospheric delay correction term in seconds with frequency f_i ($i = u$ or d) at position j which can be represented as follows:

$$I_{ij}(t) = \frac{40.3 \cdot TEC_j(t)}{c \cdot f_i^2} \quad (4)$$

$TEC_j(t)$ is the total electron content, the total number of free electrons along the signal path at position j , which is conventionally measured in TEC units, $1 \text{ TECU} = 10^{16}$ electrons/ m^2 . f_u and f_d are the uplink and downlink frequencies, respectively.

Similarly, the phase information from B to A, from A to A, and from B to B, are respectively represented by

$$\begin{aligned}\phi_{ba}(t) &= \omega_u \tau_b(t) - \omega_s \tau_s(t) - \omega_d \tau_a(t) - (\omega_u \rho_{bs}(t) + \omega_d \rho_{as}(t))/c \\ &\quad + \omega_u I_{ub}(t) + \omega_d I_{da}(t) + \omega_u T_b(t) + \omega_d T_a(t)\end{aligned}\quad (5)$$

$$\begin{aligned}\phi_{aa}(t) &= \omega_u \tau_a(t) - \omega_s \tau_s(t) - \omega_d \tau_a(t) - (\omega_u \rho_{as}(t) + \omega_d \rho_{as}(t))/c \\ &\quad + \omega_u I_{ua}(t) + \omega_d I_{da}(t) + \omega_u T_a(t) + \omega_d T_a(t)\end{aligned}\quad (6)$$

$$\begin{aligned}\phi_{bb}(t) &= \omega_u \tau_b(t) - \omega_s \tau_s(t) - \omega_d \tau_b(t) - (\omega_u \rho_{bs}(t) + \omega_d \rho_{bs}(t))/c \\ &\quad + \omega_u I_{ub}(t) + \omega_d I_{db}(t) + \omega_u T_b(t) + \omega_d T_b(t)\end{aligned}\quad (7)$$

In general, the geometrical distance from station A to the satellite and the corresponding distance from station B to the satellite are not symmetrical. As a result, there is a difference in the arrival times of signals from stations A and B at the satellite. This difference is generally a few milliseconds [19]. We assume that the onboard translation oscillator signal is stable during this time difference, and the induced phase jitter is negligible and thus consider only the one unknown τ_s in all equations (3), (5) - (7).

By subtracting equation (3) from equation (5),

$$\begin{aligned}\phi_{ab}(t) - \phi_{ba}(t) &= \omega_+(\tau_a(t) - \tau_b(t)) - \omega_-(\rho_{as}(t) - \rho_{bs}(t))/c \\ &\quad + \omega_-(T_a(t) - T_b(t)) + \omega_u(I_{ua}(t) - I_{ub}(t)) - \omega_d(I_{da}(t) - I_{db}(t)),\end{aligned}\quad (8)$$

and (6) and (7),

$$\begin{aligned}\phi_{aa}(t) - \phi_{bb}(t) &= \omega_-(\tau_a(t) - \tau_b(t)) - \omega_+(\rho_{as}(t) - \rho_{bs}(t))/c \\ &\quad + \omega_+(T_a(t) - T_b(t)) + \omega_u(I_{ua}(t) - I_{ub}(t)) + \omega_d(I_{da}(t) - I_{db}(t)),\end{aligned}\quad (9)$$

the terms related to the onboard signal are canceled. Here, $\omega_+ \equiv \omega_u + \omega_d$ and $\omega_- \equiv \omega_u - \omega_d$ apply.

In TWCP, the geometrical distances in equations (8) and (9), ρ_{as} and ρ_{bs} , are unknown. Therefore, it is necessary to further subtract these intermediate results to cancel them.

$$\begin{aligned} & \omega_+(\phi_{ab}(t) - \phi_{ba}(t)) - \omega_-(\phi_{aa}(t) - \phi_{bb}(t)) \\ &= (\omega_+^2 - \omega_-^2)(\tau_a(t) - \tau_b(t)) \\ &+ 2\omega_u\omega_d[(I_{ua}(t) - I_{ub}(t)) - (I_{da}(t) - I_{db}(t))] \end{aligned} \quad (10)$$

The time difference between stations A and B is finally computed as follows:

$$\begin{aligned} \tau_a(t) - \tau_b(t) &= \frac{\omega_+\alpha(t) - \omega_-\beta(t)}{\omega_+^2 - \omega_-^2} \\ &+ \frac{2\omega_u\omega_d}{\omega_+^2 - \omega_-^2}[(I_{da}(t) - I_{ua}(t)) - (I_{db}(t) - I_{ub}(t))] \end{aligned} \quad (11)$$

$$\begin{aligned} \alpha(t) &\equiv \phi_{ab}(t) - \phi_{ba}(t) \\ \beta(t) &\equiv \phi_{aa}(t) - \phi_{bb}(t) \end{aligned}$$

Here the tropospheric delays are canceled. On the right hand of equation (11), the first term is derived from the four observed phases, and the second one is for ionospheric delay correction. Typically, TWSTFT uses uplink and downlink frequencies of 14 GHz and 11 GHz, respectively. In this case, the coefficients of $\omega_+/(\omega_+^2 - \omega_-^2)$ and $\omega_-/(\omega_+^2 - \omega_-^2)$ become 7×10^{-12} and 8×10^{-13} , respectively. Thus, a measurement precision of 10^{-13} seconds can be expected when the phase detection has a resolution of less than 0.1 radians.

When $TEC_j(t)$ is obtained by other methods such as a theoretical model or actual measurement, the ionospheric correction term can be calculated. The ionospheric delay needs to be considered carefully because of the frequency difference between uplink and downlink and the TEC difference between the ionospheres at stations A and B. The TWCP frequencies are, however, higher than those used in GPS such that the effect due to the ionosphere (prop. $1/f^2$) is smaller than that encountered in GPS time transfer. The amplitude could be up to a few hundred picoseconds, and is assumed to be negligible in conventional TWSTFT (hereafter TWCode), but it cannot be neglected in TWCP.

3. Experimental setup

The TWCP experiment was performed using a link between NICT and Physikalisch-Technische Bundesanstalt (PTB) by employing the geostationary communication satellite AM-2 located at a longitude of 80 degrees East. The actual distance between the two sites is approximately 9,000 km, making it one of the longest baselines in the world. In parallel, TWCode measurement was performed once every hour using the same satellite that has been used to link Asian and European laboratories belonging to the TAI networks [13]. The satellite IS-4 was used for this purpose for many years.

bandwidth was limited by a 200-kHz digital filter. In addition, it had a feature to overlay 50 bps data, allowing it to identify the start of a code pattern which is synchronized with the external 1 pps, and to reduce the interference between codes. A signal with a center frequency of 70 MHz, which was generated by the AWG, was then up-converted to a higher 14 GHz frequency using a frequency up-converter (U/C). The signal was amplified by a solid-state power amplifier (SSPA) and fed to the antenna. Both stations used a different code in their transmission path.

The signal received by the antenna with a center frequency of 11 GHz was amplified by a low-noise amplifier (LNA) and down-converted to 70 MHz by a frequency down-converter (D/C). The U/C and D/C were phase locked to external 10-MHz signals. The signal passed through a band-pass filter (BPF) with a frequency bandwidth of 2 MHz, and it was amplified by an additional amplifier. Then, it was sent to an analog-to-digital (A/D) sampler. The A/D sampler was originally developed for very long-baseline interferometry (VLBI) [22]. Data sampling was performed with a sampling rate of 64 MHz in synchronized timing with the external reference signals of 10 MHz and 1 pps. After splitting the sampled data into in-phase and quadrature components, the cross correlation with a replica code, group delay, and carrier-phase detection were sequentially conducted in the computer. Each antenna received two pseudo-random noise signals, that is, the own and the one transmitted from the counterpart station. Therefore two data-processing sequences ran in parallel. The code and carrier-phase information was then written every 20 ms. Finally, the midpoint of the second-order fit to the 50 data points obtained during each second was defined as the data at that second. With the exception of the AWG and A/D sampler, the instruments were identical to those used for TWCode stations.

The PTB station was dedicated for conducting TWCP measurements; it was equipped with a 1.8-m antenna dish. The elevation angle was 3.7°. The PTB station was connected to UTC(PTB) signals of 1 pps and 10 MHz. UTC(PTB) is derived from a steered active hydrogen maser [23] and the frequency stability is at the 10^{-15} level for averaging times exceeding 10^4 seconds. Because the PTB station was located a few hundred meters away from the building in which hydrogen masers are operated and the UTC(PTB) time scale is realized, the reference signals of 10 MHz and 1 pps were distributed using a 1-km-long optical fiber link. It was confirmed that the distribution instability was sufficiently small compared to the stability of the reference signal without any fiber-length stabilization.

On the other hand, the NICT station with a 2.4-m dish was shared by the TWCode and TWCP measurements. The elevation angle was 16.0°, and both measurements were performed simultaneously. The 200-kHz and 2.5-MHz wide signals at sufficiently different carrier frequencies were generated by the AWG and a TWCode modem, respectively, and were combined after the frequency up-conversion from 70 MHz to 14 GHz to avoid the generation of inter-modulation. The received signal was split into two components after amplification by the LNA, and the two components were input into different D/Cs. The 200-kHz signal was separated from the 2.5-MHz TWCode

signal by the BPF. We confirmed that there was no degradation in the measurement precision caused by the combined processing of the two signals. The NICT station was connected to UTC(NICT) signals of 1 pps and 10 MHz. UTC(NICT) is generated from a steered active hydrogen maser and the frequency stability is at the 10^{-15} level for averaging times exceeding 10^4 seconds [24].

4. Error sources over a very long baseline

4.1. Compensation for Ionospheric delay

Because ionospheric delay is inversely proportional to the square of the signal frequency, it is not canceled out in TWSTFT because of the frequency difference between the uplink and downlink. In TWCode, it is assumed that the impact of the ionospheric delay is negligible [25]. On the other hand, it should be considerable in the TWCP link taking the high performance into account. Because the TWCP measurement is carried out by using a pair of uplink and downlink frequencies, the TEC along the signal path cannot be measured; two downlink frequencies would be needed as it is the case when a dual-frequency GPS receiver is employed. We read out the vertical total electron content (VTEC) over NICT and PTB from some VTEC maps and compensated for the ionospheric delays present in the TWCP result. The Center for Orbit Determination in Europe (CODE) [26] generates the Global Ionosphere Map (GIM) based on observations that are made at about 150 GPS sites around the world. The GIM provides VTEC maps with a time resolution of 2 h and latitude/longitude resolution of 2.5/5.0 degrees. It is assumed that the VTEC is present in an infinitely thin layer at a height of 450 km. To compute the VTEC E at latitude β , longitude λ , and universal time t , we first read out four VTEC values, $E_{0,0}$, $E_{1,0}$, $E_{0,1}$, $E_{1,1}$, at epoch T_i around the coordinates (λ, β) and perform grid interpolation:

$$\begin{aligned} E_i(\beta, \lambda) &= E_i(\lambda_0 + p\Delta\lambda, \beta_0 + q\Delta\beta) \\ &= (1-p)(1-q)E_{0,0} + p(1-q)E_{1,0} + q(1-p)E_{0,1} + pqE_{1,1}, \end{aligned} \quad (12)$$

where $0 \leq p < 1$ and $0 \leq q < 1$. $\Delta\lambda$ and $\Delta\beta$ are the grid resolutions in longitude and latitude, respectively. Then, we perform the interpolation of time using the consecutive VTEC maps:

$$E(\beta, \lambda, t) = \frac{T_{i+1} - t}{T_{i+1} - T_i} E_i(\beta, \lambda) + \frac{t - T_i}{T_{i+1} - T_i} E_{i+1}(\beta, \lambda), \quad (13)$$

where $T_i \leq t < T_{i+1}$. Next, we compute a slant TEC along the signal path from VTEC $E(\beta, \lambda, t)$ using the elevation angle z of an Earth station to a communication satellite.

$$z' = \sin^{-1} \left[\frac{R \sin(\pi/2 - z)}{R + h} \right], \quad (14)$$

$$TEC(\beta, \lambda, t) = \frac{E(\beta, \lambda, t)}{\cos z'}, \quad (15)$$

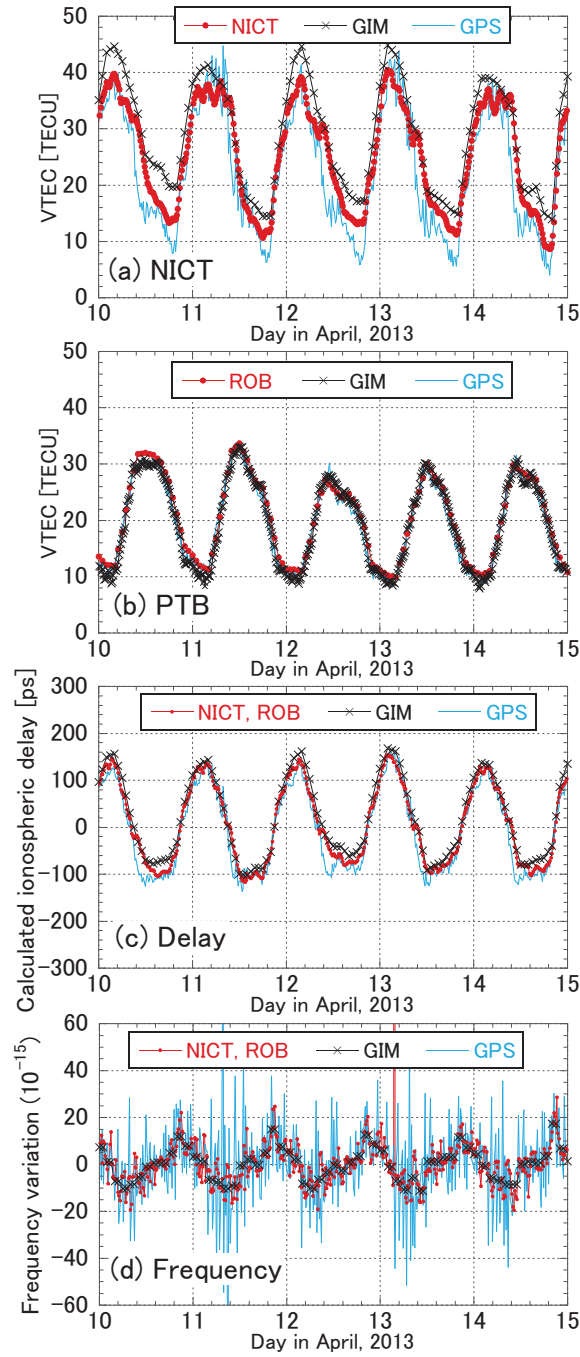


Figure 2. (a) VTEC over NICT computed from the NICT VTEC map, GIM, and GPS, (b) VTEC over PTB computed from the ROB VTEC map, GIM, and GPS, (c) calculated ionospheric delay and (d) expected frequency variation in the NICT-PTB link computed from the NICT and ROB VTEC maps, GIM and GPS.

where R is the radius of the Earth and h is the height of the ionosphere [15]. Thus, the ionospheric delay over an Earth station in TWSTFT is derived using equation (4) and $TEC(\beta, \lambda, t)$ computed from a VTEC map [27]. However, the time resolution and grid interval of the GIM are not sufficiently dense considering the TWCP measurement rate

of every second. Therefore, we adopted regional VTEC maps provided by the Royal Observatory of Belgium (ROB) [28] and NICT [29] over Europe and Japan, respectively. The ROB VTEC map is based on real-time GPS observations obtained from more than 100 sites belonging to the EUREF Permanent Network [30]. The grid interval is $(0.5^\circ, 0.5^\circ)$, and the time resolution is 15 min. On the other hand, the NICT VTEC map is generated using the GPS Earth Observation Network (GEONET) data from about 200 sites in Japan [31], and its grid interval is $(2.0^\circ, 2.0^\circ)$, while its time resolution is also 15 min.

We first evaluated the disagreement between NICT and ROB VTEC maps, and the GIM. In addition, the VTEC values were calculated from the CGGTTS data [32] of dual-frequency GPS receivers at NICT and PTB using equation (4), (14) and (15). Since the GPS receivers have multi channels, the mean values of each measurement epoch every 16 min were calculated. Figures 2 (a) and (b) show the VTEC values over NICT and PTB, which were derived from NICT and ROB VTEC maps, GIM and GPS data. Time and grid interpolation was performed as previously described. The time resolutions were every 15 min, 1 h and 16 min for the results using NICT and ROB VTEC maps, GIM, and GPS, respectively. We found that the disagreements between the NICT VTEC map and GIM was always less than 6 TECU. In addition, the maximum difference between the NICT VTEC map and the result by GPS was 7 TECU. In particular, the ROB VTEC map shows a good agreement with GIM and the result by GPS. Thus the regional VTEC maps were considered appropriate for our purpose and were employed for compensation because they had a minimum time resolution. Figure 2 (c) depicts the calculated ionospheric delays described in equation (11) and Figure 2 (d) shows the converted frequency variations whose data spacing is 15 min. The result by GPS shows a larger frequency deviation, however, the mean value looks consistent with those by GIM and the regional VTEC maps. Depending on the VTEC maps utilized, no significant differences were observed. The amplitudes exceeding 100 ps are caused by amplification of the effect due to the local time difference between Japan and Germany and the low elevation angle at the PTB station. However, such a local time difference and low elevation angle are unavoidable over a very long baseline.

4.2. Other sources

The possible delay sources over a very long baseline are listed in Table 2. With the exception of ionospheric delay, these error sources are roughly estimated in this subsection. In our description of the time difference using carrier-phase information, it is assumed that the induced phase jitter during frequency conversion at the satellite transponder is negligible; however, the impact is actually unknown. We previously evaluated phase jitters caused by instruments [11]. From our results, it was determined that a jitter of 0.2 ps caused by a commercially available frequency converter is the largest in the TWCP system. The temperature coefficients of the instruments were also measured using a temperature-controlled bath. We confirmed that a commercially

Table 2. Delay sources over a very long TWCP link.

Item	Amplitude in time [ps]
phase jitter in satellite transponder	unknown
phase jitter in instruments	0.2 (frequency converter)
phase variation in instruments	100
ionosphere	100
troposphere	3
Sagnac effect	10 to 150
2nd order Doppler shift	2

available frequency converter had the largest value of about ± 700 ps/K. As shown in the next section, outdoor instruments can also cause phase variations. The phase variation caused by a temperature variation would be considerable, depending on magnitude and period. We estimate that this effect to be 200 ps peak-to-peak at maximum.

The tropospheric delay is normally assumed to be frequency independent up to frequencies slightly above 10 GHz, and it is believed that it is canceled out in TWSTFT. However, in principle, the troposphere refraction index is dependent on frequency, and it induces a small impact in TWSTFT. As shown in equation (11), the delays that are dependent on the frequency are coupled with the ionosphere delays, and they induce phase variation. Piester et al. estimated a peak-to-peak amplitude of 2 ps for the NICT-PTB link in the case involving IS-4 [33]. Considering the difference in the elevation angles, it may attain a peak-to-peak of 5 ps in the case involving the AM-2 satellite currently used. When there is such a delay variation within a 24-h period, it is equivalent to an increase of the Allan deviation by 10^{-16} at half day averaging time calculated as 5×10^{-12} s/43200 s. This magnitude can still be considered to be smaller than other error sources.

The Sagnac effect is caused by the rotation of the Earth and it induces a propagation time difference between two stations. TWSTFT is generally performed using a geostationary satellite. A delay correction is routinely done in TWCode, assuming that the propagation time difference is constant. Because of slight movements around the central position of the satellite, the difference in the propagation time, however, has a periodic daily variation. The amplitude of the time difference depends on the position of the Earth station and the magnitude of the movement of the satellite. We computed the satellite position using the two line elements (TLE) published by the North American Aerospace Defense Command (NORAD) [34] and estimated the time difference due to the Sagnac effect. The amplitudes of the time difference due to the Sagnac effect in the NICT-PTB link obtained using the IS-4 satellite varied from several hundred picoseconds to several tens of picoseconds, depending on the satellite's orbit. On the other hand, amplitudes of only some tens of picoseconds were computed in the case involving the AM-2 satellite. Evidently, the position of the AM-2 satellite is more tightly controlled than that of the IS-4 used to be. Here, we do not take this correction

into account.

In equation (3), the term of the second order Doppler shift $v_a/c \cdot v_b/c$ is negligible. We measured the magnitudes of v/c using the IS-4 and AM-2 satellites, which had a maximum value of 10^{-9} and less than 10^{-8} , respectively. Thus, it is thought that the term induces a maximum instability of 10^{-16} with a diurnal pattern. Accordingly, we estimated an amplitude of 2 ps, and we do not consider a correction.

4.3. Environmental effect

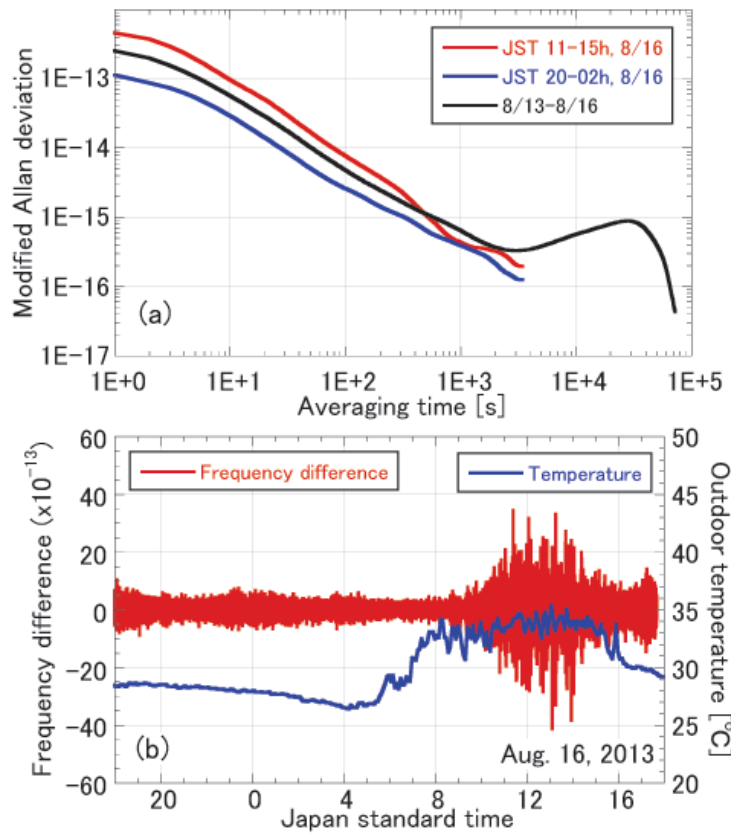


Figure 3. (a) TWCP instabilities and (b) frequency difference with the outdoor temperature in the common clock measurement at NICT.

During TWCP measurements, we observed some phenomena that may have been related to the outdoor instruments and temperature. Transmission power decreased by about 10 dB when the outdoor temperature at PTB increased to more than 30 $^{\circ}\text{C}$. The measurement precision of TWCP degraded by a factor of 4 during the daytime, as shown in Figure 3, when the outdoor temperature was above 30 $^{\circ}\text{C}$ at NICT. There were little changes in the transmission power. The former occurred in June 2013 at PTB, while the latter occurred during the common clock measurement using two antenna dishes performed at NICT in August 2013. We checked the output power levels of the indoor instruments and confirmed that they had not changed in both cases.

For the former case, one possible explanation is that the SSPA (see Figure 1) was affected by the heat, and the gain subsequently decreased. After the SSPA was shielded from direct sunlight, the gain recovered within a few hours. Phase variations were also observed.

For the common clock measurement in the latter case, in particular, there was a daily variation with an amplitude of about 20 ps, and it had a correlation with the variation of the outdoor temperature. Besides, the short-term instability observed during the daytime was clearly degraded compared to that in the nighttime, as shown in Figure 3 (a). Because the LNA was temperature-stabilized and the indoor temperature did not vary much at the NICT station, it is thought that the outdoor temperature rise caused the phase jitter to increase. We concluded that more attention should be paid to the condition of the outdoor instruments. In particular, in the case of a very long baseline, the phase variation attributed to the temperature variation may be enlarged by the local time difference. It would be required to avoid heating and temperature variations on the installed equipment to fully utilize the performance of TWCP.

5. Link performance

5.1. Time and frequency transfer

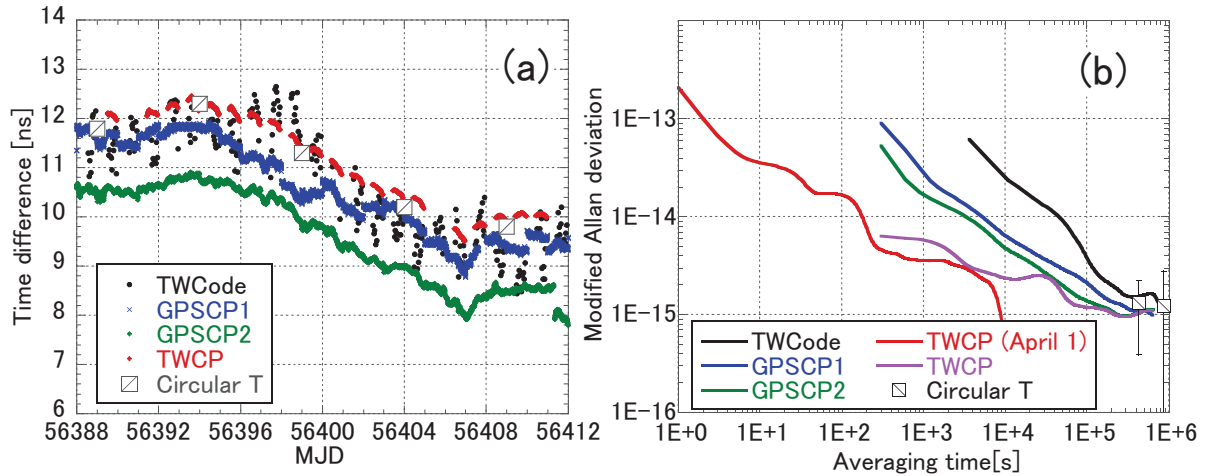


Figure 4. (a) Time difference between UTC(NICT) and UTC(PTB) in April 2013, (b) Frequency instabilities measured by TWCode, GPSCP and TWCP. The frequency instabilities by TWCP in red line and purple line were achieved for a short period of one day in April 1 and a long period of one month in April, respectively.

The TWCP experiment was performed from March to June 2013 and the time difference between UTC(NICT) and UTC(PTB) was measured. The result was compared with those achieved by TWCode and GPSCP for the evaluation. The GPS receivers that were used are listed in Table 3, and they performed dual-frequency code

Table 3. GPS receivers used for the NICT-PTB link.

Caption	Receiver at PTB	Receiver at NICT
GPSCP1	ASHTECH Z-XII3T	Septentrio PolaRx2 TR
GPSCP2	ASHTECH Z-XII3T	ASHTECH Z-XII2T

and phase measurements recorded in RINEX 2.1 format. There were measurement gaps in the TWCP and TWCode results because of the limited working time of the satellite transponder between 12:00 UTC and 22:00 UTC. The phase discontinuity in the TWCP was filled by an integral multiple of a number to fit the result of GPSCP2. The numbers of the cycle slips in the phase information $\phi_{ab}, \phi_{ba}, \phi_{aa}, \phi_{bb}$ are assumed as $n_{ab}, n_{ba}, n_{aa}, n_{bb}$, which are not necessarily the same because the phase information are detected by two independent data-processing sequences at two stations. With the amplitude $A = 1/(\omega_+^2 - \omega_-^2)$, the offset t_N in time due to the cycle slips is written as $t_N = A[(n_{ab} - n_{ba})\omega_+ - (n_{aa} - n_{bb})\omega_-] = A(n\omega_+ - m\omega_-)$. Here n and m are arbitrary integers. Since the minimum resolution of t_N is $A\omega_-$, an integral multiple of $A\omega_-$ is used to fill a gap in a TWCP result. In the subsequent case, it was about 0.8 ps.

Figure 4(a) shows the measurement results obtained using TWCode, GPSCP1, GPSCP2, and TWCP. Offset values are applied into the plot for better visibility. The TWCode measurement was performed once every hour. In each measurement, the midpoint of the second-order fit for 5 min (300 data points) was calculated. The TWCP measurement was continuously performed while the transponder was available, where data were taken every second. The mean values over 5 min are depicted in Figure 4. The GPSCP results were computed every 5 min as well [35]. The white squares indicate the time difference published in the Circular T 304 [36]. The time link between PTB and NICT adopted for TAI is built on GPSPPP, and the same receiver data are used by BIPM as in this study. It is clear that the TWCP results agree with that of TWCode within the large dispersion of the TWCode data. On the other hand, TWCP and GPSCP2 show a good agreement because the phase ambiguity in the TWCP result was compensated to fit to GPSCP2. Further, it appears that it is also almost consistent with GPSCP1. A detailed comparison between GPSCP and TWCP is discussed in the next subsection. Figure 4(b) shows their frequency instabilities presented in the modified Allan deviation, which were from April 1 to April 30, 2013. The TWCP instabilities that were both measured on April 1, 2013 and 300 s averaged from April 1 to April 30 were depicted. We confirmed that an instability of 2×10^{-13} at 1 s was possible by TWCP over such a very long baseline. The instability obtained by TWCP reaches a level below 10^{-14} after an average time of 200 s. On the other hand, those obtained by GPSCP2 and TWCode reached the same level only after 3600 s and 46800 s, respectively. At observation times exceeding one day, the comparisons are limited by the combined frequency instability of the two time scales/clocks involved at NICT and PTB. Therefore a detailed analysis using double differences is given in the following

section.

5.2. Comparison with GPSCP

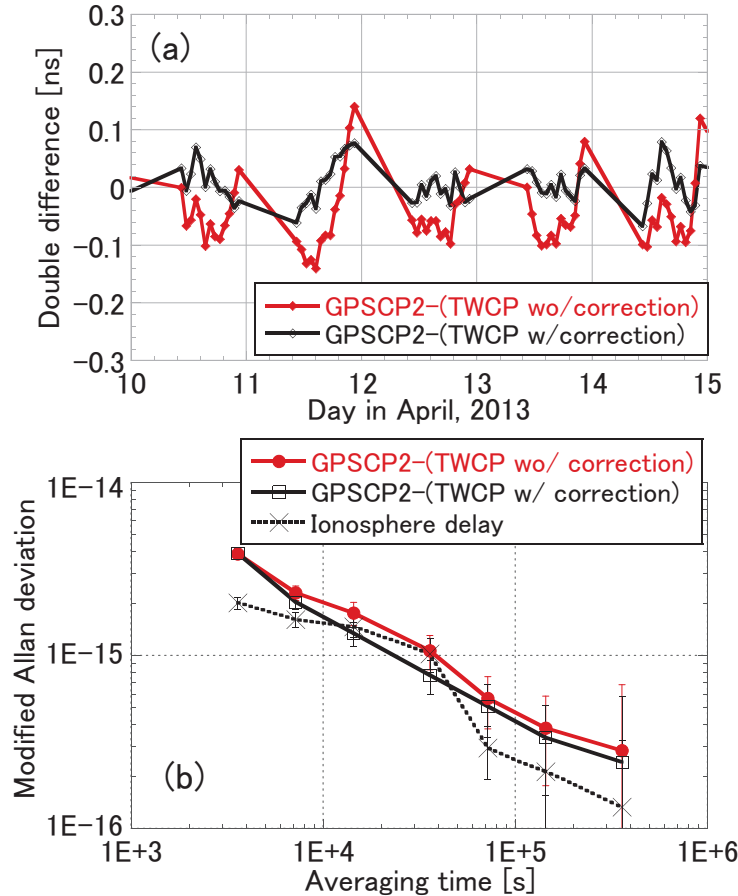


Figure 5. (a) 1-h averaged double difference of the NICT-PTB link between GPSCP2 and TWCP with and without ionospheric compensation and (b) modified Allan deviation.

In order to characterize the NICT-PTB link performance, double differences between GPSCP and TWCP solutions are formed which should be free of clock noise. Figure 5(a) shows the double differences in delay between GPSCP2 and TWCP with and without ionospheric compensation. The data were averaged for 1 h and then subtracted. Here GPSCP1 and GPSCP2 are ionosphere free. The data of GPSCP1 were not adopted in the plot because there were some discontinuities. As shown in Figure 2(c), the ionospheric delay has its maximum close to 0:00 UTC. Therefore, the disagreement between GPSCP2 and TWCP follows a similar signature. However, it was improved by compensating for the ionospheric delay. The achieved frequency instabilities expressed by the modified Allan deviation are depicted in Figure 5(b), and the 10^{-16} level is reached after 40000 s. Those having the ionospheric compensation show slightly better values. The dashed line shows the impact due to the ionospheric delay in the NICT-PTB

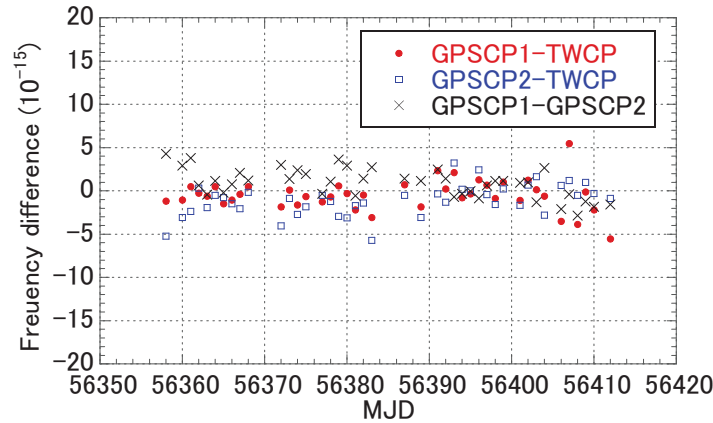


Figure 6. Frequency differences for combinations of GPSCP1, GPSCP2 and TWCP. They are averaged for 1 day (10 hours). Data of GPSCP and TWCP are plotted only when both kinds were available.

TWCP link, which is at the low 10^{-16} level for an averaging time of one day. From this result, we deduce that averaging for longer than one day will be effective for reducing the influence in the case that 24-h continuous measurements will be possible.

The frequency differences for GPSCP1-TWCP, GPSCP2-TWCP, and GPSCP1-GPSCP2 are shown in Figure 6 (1-day from 12:00 to 22:00 average values). Outliers exceeding three times the standard deviation were previously removed. In the TWCP results, we compensated for the ionospheric delay. Their differences in March and April 2013 are listed in Table 4. Without the ionospheric compensation, the values of GPSCP1-TWCP and GPSCP2-TWCP are 1.24×10^{-15} and 1.44×10^{-15} , respectively. From these results, it is clear that compensation leads to improved consistency. The difference between GPSCP1 and GPSCP2 was caused by the GPS receiver used at NICT. When we limited the data's available time from 12:00 to 22:00 in UTC, that is, the satellite transponder working time, the frequency difference between GPSCP1 and GPSCP2 became larger. From this result, the limited measurement period may have contributed to the difference in frequency. In other words, any error source that exists with daily variations may remain in both TWCP and GPSCP. As a result, a frequency offset may be induced by limiting the measurement time. We used the regional VTEC maps to compensate for the ionospheric delay; we have to evaluate their uncertainties more carefully. Besides, other error sources should be considered to reduce the daily variation. From Table 4, we concluded that the systematic uncertainty in frequency comparisons via the TWCP link was less than 1×10^{-15} .

6. Conclusion

We performed a TWCP experiment between NICT and PTB, and we confirmed that TWCP is possible over very long baselines, ranging up to about 9,000 km. The result showed a good agreement with those measured by TWCode and GPSCP, and a short-

Table 4. Frequency differences in March and April 2013 ($\times 10^{-15}$).

Caption	Frequency difference	Standard uncertainty	No. of points
GPSCP1-TWCP (12-22h)	-0.56	0.33	446
GPSCP2-TWCP (12-22h)	-0.95	0.32	453
GPSCP1-GPSCP2 (full day)	0.47	0.19	1257
GPSCP1-GPSCP2 (12-22h)	0.79	0.28	442

term instability of 2×10^{-13} at 1 s was achieved. It is clear that the measurement precision is superior to that of TWCode and GPSCP, and it is independent of the baseline length. On the other hand, the effect of the ionospheric delay is more noticeable over a long baseline. We computed the ionospheric delays using the local VTEC maps provided by ROB and NICT and found that the amplitude reached about 100 ps. The disagreement between TWCP and GPSCP was decreased by the compensation. The modified Allan deviation of GPSCP-TWCP was improved and reached the 10^{-16} level. Meanwhile, there remains a frequency disagreement between them at the 10^{-16} level. One possible explanation is that there is an instability due to a daily variation, which induced the frequency offset caused by the limited measurement time. The long-term instability should be further evaluated by performing a 24-h operation. In addition, it may be necessary to improve the environment in which the instruments are installed, when the high performance of TWCP shall be utilized.

Acknowledgments

We would like to thank H. Maeno and R. Tabuchi at NICT for their assistance with establishing the link. We would also like to thank P. Defraigne at ROB and M. Nishioka at NICT for the information regarding the regional VTEC maps.

References

- [1] E. Peik and A. Bauch, “More Accurate Clocks - What are They Needed for?”, Special Issue / PTB-Mitteilungen, **119**, pp. 16-24, 2009.
- [2] E. Peik, “Fundamental constants and units and the search for temporal variations”, Nuclear Physics B (Proc. Suppl.), 203-204, pp. 18-32, 2010.
- [3] J. Frisch, D. Bernstein, D. Brown, and E. Cisneros, “A high stability, low noise RF distribution system”, in Proc. Particle Accelerator Conf. 2002, vol. 2, 2002, pp. 816-818.
- [4] P. Krehlik, L. Sliwczynski, L. Buczek, and M. Lipinski, “Fiber-Optic Joint Time and Frequency Transfer With Active Delay Stabilization of the Propagation Delay”, IEEE Trans on Instr. Measurement, vol. 61, no. 10, 2844-2851, 2012.
- [5] M. Rost, D. Piester, W. Yang, T. Feldmann, T. Wübbena, A. Bauch, “Time transfer through optical fibers over a distance of 73 km with uncertainty below 100 ps”, Metrologia, vol. 49, no. 6, pp. 772-778, 2012.
- [6] O. Lopez, A. Kanji, P.-E. Pottie, D. Rovera, J. Achkar, C. Chardonnet, A. Amy-Klein, G. Santarelli, “Simultaneous remote transfer of accurate timing and optical frequency over a public fiber network”, J. Appl. Phys. B. vol. 110, no. 1, pp. 3-6, 2013.

- [7] White Rabbit project: <http://www.ohwr.org/projects/white-rabbit>.
P. Moreira, J. Serrano, T. Wolstowski, P. Loschmidt, and G. Gaderer, "White rabbit: Sub-nanosecond timing distribution over Ethernet", ISPCS 2009 International Symposium on Precision Clock Synchronization for Measurement, Control and Communication, pp. 58-62, 2009.
- [8] A. Yamaguchi, M. Fujieda, M. Kumagai, H. Hachisu, S. Nagano, Y. Li, T. Ido, T. Takano, M. Takamoto, and H. Katori, "Direct Comparison of Distant Optical Lattice Clocks at the 10^{-16} Uncertainty", *Applied Physics Express* 4, 082203, 2011.
- [9] A. Matveev et al., "Precision Measurement of the Hydrogen 1S-2S Frequency via a 920-km Fiber Link", *Phys. Rev. Lett.* 110, 23081, 2013.
- [10] K. Predehl, G. Grosche, S. M. F. Raupach, S. Droste, O. Terra, J. Alnis, Th. Legero, T. W. Hansch, Th. Udem, R. Holzwarth, H. Schnatz, "A 920-Kilometer Optical Fiber Link for Frequency Metrology at the 19th Decimal Place", *Science* vol. 336, 441-444, 27 APRIL 2012.
- [11] M. Fujieda, T. Gotoh, F. Nakagawa, R. Tabuchi, M. Aida, and J. Amagai, "Carrier-Phase-Based Two-Way Satellite Time and Frequency Transfer", *IEEE Trans. Ultrason. Ferroelectr. Freq. Control*, vol. 59, no. 12, 2625-2630, 2012.
- [12] D. Piester, H. Schnatz, "Novel techniques for remote time and frequency comparisons", *PTB-Mitteilungen*, vol. 119, pp. 33-44 (Special issue), 2009.
- [13] G. Panfilo and E. F. Arias, "Algorithms for International Atomic Time", *IEEE Trans. Ultrason. Ferroelectr. Freq. Control*, vol. 57, no. 1, pp. 140-150, 2010.
- [14] D. Kirchner, "Two-way satellite time and frequency transfer (TWSTFT): principle, implementation, and current performance," *Rev. of Radio Science*, Oxford University Press, pp. 27-44, 1999.
- [15] A. Kleusberg, "Atmospheric Models from GPS", section 15, *GPS for geodesy*, 2nd edition, Berlin: Springer, 1998.
- [16] D. Piester, A. Bauch, J. Becker, E. Staliuniene, and C. Schlunegger, "On Measurement Noise in the European TWSTFT Network", *IEEE Trans. Ultrason. Ferroelectr. Freq. Control*, vol. 55, no. 9, pp. 1906-1912, 2008.
- [17] W. Schäfer, A. Pawlitzki, and T. Kuhn, "New Trends in Two-Way Time and Frequency Transfer via Satellite", in *Proc. 31th Annual Precise Time and Time Interval (PTTI) Meeting*, pp. 505-514, 1999.
- [18] B. Fonville, D. Matsakis, A. Pawlitzki, W. Schäfer, "Development of Carrier-phase-based Two-way Satellite Time and Frequency Transfer (TWSTFT)", in *Proc. 36th Annual Precise Time and Time Interval (PTTI) Meeting*, pp. 149-164, 2004.
- [19] T. E. Parker and V. Zhang, "Sources of Instabilities in Two-Way Satellite Time Transfer", in *Proc. IEEE Int. Freq. Control Sympo. and 37th Annual Precise Time and Interval (PTTI) Meeting*, pp. 745-751, 2005.
- [20] J. Amagai and T. Gotoh, "Development of Two-Way Time and Frequency Transfer System with Dual Pseudo Random Noises", *Journal of the National Institute of Information and Communications Technology*, Vol. 57, Nos. 3/4, pp.197-207, 2010.
- [21] T. Gotoh, J. Amagai, T. Hobiger, M. Fujieda, and M. Aida, "Development of a GPU-Based Two-Way Time Transfer Modem", *IEEE Trans. Instr. Meas.*, vol. 60, no. 7, pp. 2495-2499, 2011.
- [22] T. Kondo, Y. Koyama, R. Ichikawa, M. Sekido, E. Kawai, M. Kimura, "Development of the K5/VSSP system", *J. Geodetic Soc. Japan*, vol. 54, no.4, pp. 233-248, 2008.
- [23] A. Bauch, S. Weyers, D. Piester, E. Staliuniene and W. Yang, "Generation of UTC(PTB) as a fountain-clock based time scale", *Metrologia*, vol. 49, pp. 180-188, 2012.
- [24] F. Nakagawa, Y. Hanado, H. Ito, N. Kotake, M. Kumagai, K. Imamura, and Y. Koyama, "Summary and Improvement of Japan Standard Time Generation System", *Journal of the National Institute of Information and Communications Technology*, vol. 57, Nos. 3/4, pp. 17-27, 2010.
- [25] A. Bauch, D. Piester, M. Fujieda, W. Lewandowski, "Directive for operational use and data handling in two-way satellite time and frequency transfer (TWSTFT)", *Rapport BIPM-2011/01*,

- 2011.
- [26] http://www.aiub.unibe.ch/content/research/satellite_geodesy/code_research/index_eng.htm
- [27] S. Schaer and W. Gurtner, "IONEX: The IONosphere Map EXchange Format Version 1", Proc. of the IGS AC Workshop, Darmstadt, Germany, February 9-11, 1998.
- [28] http://www.gnss.be/Atmospheric_Maps/ionospheric_maps.php
N. Bergeot, J.-M. Chevalier, L. Benoit, C. Bruyninx, J. Legrand, E. Pottiaux, Q. Baire, P. Defraigne, "Near Real Time Ionosphere Models from European Permanent Network GPS Data", EUREF Annual Sym, 24-27/05/2011, Chisinau, Moldova.
- [29] <http://wdc.nict.go.jp/IONO/gps-tec/tecv/>
G. Ma and T. Maruyama, "Derivation of TEC and estimation of instrumental biases from GEONET in Japan", Ann. Geophys., pp. 2083-2093, 2003.
- [30] <http://epncb.oma.be>
- [31] S. Miyazaki, T. Saito, M. Sasaki, Y. Hatanaka, and Y. Iimura, "Expansion of GSI's nationwide GPS array", Bull. Geogr. Surv. Inst., no. 43, pp. 23-34, 1997.
Geographical Survey Institute, Japan, "GEONET (GPS Earth Observation Network System) and its Prospect", Journal of the Geodetic Society of Japan, Vol. 50, No. 2, pp. 53-65, 2004. (in Japanese)
- [32] D.W. Allan and C. Thomas, "Technical Directives for Standardization of GPS Time Receiver Software", Metrologia, vol. 31, pp. 67-79, 1994.
- [33] D. Piester, A. Bauch, M. Fujieda, T. Gotoh, M. Aida, H. Maeno, M. Hosokawa and S. H. Yang, "Studies on Instabilities in Long-baseline Two-way Satellite Time and Frequency Transfer (TWSTFT) Including a Troposphere Delay Model", Proc. of 39th Annual Precise Time and Interval (PTTI) Meeting, pp. 211-222, 2007.
- [34] <http://celestrak.com/NORAD/documentation/tle-fmt.asp>
- [35] T. Gotoh, M. Fujieda, J. Amagai, "Comparison study of GPS carrier phase and two-way time and frequency transfer", Proc. of Joint EFTF and IFCS, 2007.
- [36] <ftp://ftp2.bipm.org/pub/tai/publication/cirt/cirt.304>